AIAA 99-3770

Vorticity Dynamics in a Porous Channel of the Closed-Closed Type. Part II: A Space-Reductive Perturbation Technique

Joseph Majdalani
Marquette University
Milwaukee, WI 53233

Tae-Seong Roh
California Institute of Technology
Pasadena, CA 91125

30th AIAA Fluid Dynamics Conference
18 June–1 July 1999
Norfolk, VA

Vorticity Dynamics in a Porous Channel of the Closed-Closed Type. Part II: A Space-Reductive Perturbation Technique

J. Majdalani*
Marquette University, Milwaukee, WI 53233

T. S. Roh†
California Institute of Technology, Pasadena, CA 91125

A new multiple scale technique is applied to the linearized momentum equation arising in the context of a fluid performing small oscillations about the mean base flow in a channel with porous walls. In extracting a time-dependent formulation for the ensuing velocity field, the celebrated Taylor solution is assumed for the undisturbed state associated with large wall injection. The mathematical procedure is based on introducing two virtual scales in space: a base and an undetermined, arbitrary scale. The latter is left unspecified during the derivation process until flow parameters are constructed. Physical arguments are later invoked to define the undetermined scale, –which could not have been conjectured *a priori*. The resulting 'undetermined scale solution' offers numerous advantages. Its leading order term is simpler, shorter, and more accurate than any previous formulation. Most of all, it clearly unveils the relationship between physical parameters that decree the final motion, and provides unambiguous means to quantify the corresponding vortical wave amplitude, rotational depth of penetration, near-wall velocity overshoot, and surfaces of constant phase. In particular, it discloses a viscous parameter that has a strong influence on the depth of penetration, and furnishes a closed form expression for the maximum penetration depth in any oscillation mode. These unexpected findings open new avenues and possibilities to thoroughly quantify the location of the shear layer and accompanying penetration depth. By way of theoretical verification, comparisons to a rigorously tested regular perturbation formulation are gratifying. The most striking result is, perhaps, the completely satisfactory agreement found between asymptotic predictions and newly acquired data obtained from numerical simulations of the full, nonlinearized, Navier-Stokes equations.

I. Introduction

THE fate of shear layers in well-established flows remains a major topic in fluid mechanics that has drawn considerable attention in the past. Almost every conceivable prototypical flow has undergone much scrutiny in this manner, including channel flows with porous walls. Indeed, numerous boundary layer studies have been undertaken in conjunction with various approximate solutions to the well-known Berman equation. Examples abound in the literature and the interested reader is invited to consult the references cited in the companion paper (Majdalani, J., "Vorticity Dynamics in a Porous Channel of the Closed-Closed Type. Part I: A Regular Perturbation Technique, AIAA Paper 99-3769, hereafter named Paper I).

When harmonic pressure disturbances are superimposed on the steady field of a channel with porous walls, a rich vortical structure can be expected, as discussed in Paper I. To complete our flow field investigation, we extend our previous work by devising alternative formulations that have the capability of elucidating the boundary layer structure and emerging flow features. To that end, we develop a more sophisticated and general strategy, based on WKB and multiple

*Assistant Professor, Department of Mechanical and Industrial Engineering. Member AIAA.
†Post-Doctoral Scholar, Mechanical Engineering and Jet Propulsion Center. Member AIAA.

scale theories, to obtain greater accuracy and shorter representation of the velocity field. In the process, we introduce a space-reductive procedure that holds advantages over our former perturbation solution set out in Paper I. The main objectives are therefore both dual and interlaced: to present alternative asymptotic procedures, and to elucidate the nature of the boundary layer, whose predicament is possible in light of the new formulations.

The scheme to be followed is well-conceived. Contrary to our previously used methodology, instead of working with the vorticity transport equation, we shall extrude the velocity directly from the momentum equation. This can be accomplished in Sec. II via separation of variables but will result in a singular ordinary differential equation. We proceed thereafter by expanding the separated equation via standard WKB and two-variable multiple scales. In principle, the method of multiple scales is both powerful and straightforward since the leading-order term is usually more compact and accurate than its counterpart arrived at using other perturbative schemes. The improved accuracy can be ascribed to multiple scale formalism which draws information from the first order solution in constructing the zero order term. In practice, nonetheless, the technique can be very involved because it presupposes the knowledge of the modified scales associated with the boundary layer structure. The current problem is, in fact, exacerbated by the presence of injection at the walls.

As pointed out by Proudman,[1] a shear layer can only exist on a porous boundary when fluid is extracted therefrom. When injection is present, Catheral[2] explains how the viscous shear layer is pushed a distance from the wall in a manner to delineate two regions of virtually inviscid flow: the first being the axially drifting main stream, and the second consisting of the incoming fluid. The added difficulty, according to Proudman,[1] stems from the inability to predict, *a priori*, the free-floating position of the viscous layer. This viewpoint is shared by numerous authors, including Cole and Aroesty,[3] in their classic treatment of the 'blowhard' problem over a porous plate. Qualitatively, we know from Terrill[4] that the viscous layer draws nearer to the core with successive increases in the cross-flow Reynolds number R. The size of the layer is also confirmed in several investigations to be of $\mathcal{O}(1/\sqrt{R})$. Thus it becomes more difficult to capture the layer for large values of R. To avoid embarking on wasteful endeavors, we shall adopt the concept of penetration depth to denote the rotational region extending from the wall to the shear layer. The penetration depth, which is sometimes confused with the boundary layer thickness, defies in this problem Prandtl's classic usage of the word, which is usually restricted to flows where the dependence on the kinematic viscosity is consistent with conventional knowledge.

Reverting back to our proposed strategy, it is clear that more than a standard inner coordinate transformation is necessary here. The presence of a blown-off shear layer is usually commensurate with an intricate scale constitution that involves a triple-deck of inner, outer, and intermediate scales. For this and other technical reasons, we opt to choose an undetermined coordinate transformation to begin with. At the conclusion of the asymptotic analysis, this unspecified transformation will be determined from physical arguments. At that juncture, it will become clear why the unspecified scale could not have been guessed beforehand. It may be worthwhile mentioning that the leading-order WKB solution, that we develop early on, will be recoverable from the one-term multiple scale expression when smaller order quantities are ignored in the latter.

As we insist on thorough verifications, results from the multiple scale solution are compared with the former solution of Paper I in Sec. III. This is accompanied by comparisons with computational data retrieved from numerical simulations of the nonlinear Navier-Stokes equations. Having established a high level of confidence in the asymptotic formulations, the Richardson velocity overshoot factor is evaluated in both magnitude and location. The penetration depth is also quantified. The error associated with the multiple scale expansion is computed and compared to its precursor in Paper I. Lastly, we recapitulate and conclude our analysis in Sec. IV.

II. Mathematical Formulation

A. Separation of Variables

In Paper I, the rotational velocity was produced from the vorticity and vorticity transport equations following a number of successive approximations. Here, we shall extract $\tilde{u}$ directly and explicitly from the momentum equation, written to $\mathcal{O}(M)$. Using the same notation as before, we rearrange (4.14) of Paper I into

$$x\frac{\partial \overline{u}}{\partial x} = \tfrac{2}{\pi} S \csc(\tfrac{\pi}{2} y)$$

$$\times\left\{\left[\mathrm{i}-\tfrac{\pi}{2}\sigma\sin(\tfrac{\pi}{2}y)\right]\overline{u}-\sigma\cos(\tfrac{\pi}{2}y)\frac{\partial\overline{u}}{\partial y}+\varepsilon\frac{\partial^2\overline{u}}{\partial y^2}\right\}. \quad (2.1)$$

We then call for separation of variables in order to investigate a solution of the type

$$\overline{u}(x,y)=X(x)Y(y)\,. \quad (2.2)$$

Inserting (2.2) back into (2.1), and setting $\theta=\frac{\pi}{2}y$ renders,

$$\frac{2S}{\pi Y}\csc(\theta)\left\{\left[\mathrm{i}-\tfrac{\pi}{2}\sigma\sin(\theta)\right]Y-\sigma\cos(\theta)\frac{\mathrm{d}Y}{\mathrm{d}y}+\varepsilon\frac{\mathrm{d}^2Y}{\mathrm{d}y^2}\right\}$$
$$=\frac{x}{X}\frac{\mathrm{d}X}{\mathrm{d}x}=\lambda_n\,, \quad (2.3)$$

where λ_n must be strictly positive for a nontrivial outcome. For every λ_n, a solution X_n and Y_n must be realized. Integration of the axially dependent equation is straightforward. The exact result is $X_n(x)=c_n x^{\lambda_n}$, where c_n is a simple integration constant. Owing to the linearity of (2.1), the general solution takes the form

$$\overline{u}(x,y)=\sum_{\lambda_n}c_n x^{\lambda_n}Y_n(y)\,, \quad (2.4)$$

where Y_n must be determined from the no-slip boundary condition at the wall that is chiefly responsible for the strong coupling between pressure and vorticity modes. As a consequence of this, rotational and irrotational components of the axial velocity must be equal and opposite at the wall. This is fulfilled when, $\tilde{u}=-\hat{u}$, or

$$\overline{u}(x,0)=-\mathrm{i}\sin(k_m x)\,. \quad (2.5)$$

Inserting (2.5) into (2.4), writing out the MacLaurin series expansion for the Sine function, and equating summation terms yields

$$\sum_{\lambda_n}c_n x^{\lambda_n}Y_n(0)\equiv-\mathrm{i}\sum_{n=0}^{\infty}\frac{(-1)^n(k_m x)^{2n+1}}{(2n+1)!}, \quad (2.6)$$

which will be true if, for integral values of n,

$$\lambda_n=2n+1,,\quad c_n=-\mathrm{i}\frac{(-1)^n(k_m)^{2n+1}}{(2n+1)!}, \quad (2.7)$$

$$Y_n(0)=1\,, \quad (2.8)$$

turning (2.4) into

$$\overline{u}(x,y)=-\mathrm{i}\sum_{n=0}^{\infty}\frac{(-1)^n(k_m x)^{2n+1}}{(2n+1)!}Y_n(y)\,. \quad (2.9)$$

Finally, the velocity eigenfunction Y_n is left to be determined from (2.3), viz.

$$\varepsilon\frac{\mathrm{d}^2Y_n}{\mathrm{d}y^2}-\sigma\cos\theta\frac{\mathrm{d}Y_n}{\mathrm{d}y}+\left[\mathrm{i}-\tfrac{\pi}{2}\sigma(1+\lambda_n)\sin\theta\right]Y_n=0 \quad (2.10)$$

which must satisfy the two existing boundary conditions:

$$Y_n(0)=1\,,\text{ and }\frac{\mathrm{d}Y_n(1)}{\mathrm{d}y}=0\,. \quad (2.11)$$

Unfortunately, (2.10) does not possess an exact, closed-form solution. The presence of a small multiplier in the highest derivative suggests, however, the possibility of a perturbation treatment. Due to the oscillatory solution behaviour, both WKB and two-variable multiple scale expansions appear to hold promise. In fact, the latter technique has been shown by Majdalani[5] to result in partially valid local solutions corresponding to outer, inner, and intermediate scales. In the same work, a uniform two-scale expansion was presented using a hybrid technique. The technique was based on the choice of a so-called 'composite scale' that reproduced the inner, outer, and transition scales in their respective domains. Instead of constructing the composite scale from our foreknowledge of inner, outer, and modified scales, we now attempt a different route to determine the necessary scaling transformation.

B. The WKB Approach

In searching for an asymptotic solution to the boundary value problem set out in (2.10)-(2.11), two cases may arise depending on the order of the Strouhal number.

1. *The Outer Expansion*

For small Strouhal numbers, $\sigma=\mathcal{O}(1)$, and the leading-order term of the outer solution Y_n^o can be obtained straight-forwardly from

$$-\sigma\cos\theta\frac{\mathrm{d}Y_n^o}{\mathrm{d}y}+\left[\mathrm{i}-\tfrac{\pi}{2}\sigma(1+\lambda_n)\sin\theta\right]Y_n^o=0\,. \quad (2.12)$$

Fulfillment of $Y_n(0)=1$ gives

$$Y_n^o=[\cos(\tfrac{\pi}{2}y)]^{\lambda_n+1}\exp\left\{\tfrac{2}{\pi}\mathrm{i}S\ln\tan\left[\tfrac{\pi}{4}(1+y)\right]\right\}$$
$$\equiv(\cos\theta)^{2n+2}\exp(\tfrac{2}{\pi}\mathrm{i}S\mathrm{gd}^{-1}\theta). \quad (2.13)$$

where gd^{-1} is the inverse Gudermannian function. Since the cosine factor in Y_n^o decays rapidly as $y\to1$, the other boundary condition at the core is self-satisfied by the first derivative. This eliminates the need for an inner solution at this order. On a separate note, the exponential term in Y_n^o denotes an oscillatory behavior that is commensurate with the size of S. The first order correction can be found in a similar fashion. The resulting outer solution, at $\mathcal{O}(\varepsilon^2)$, is

$$Y_n^o=(\cos\theta)^{2n+2}\exp(\tfrac{2}{\pi}\mathrm{i}S\mathrm{gd}^{-1}\theta)(1$$
$$-\varepsilon S\{\tfrac{1}{\pi}S^2(\mathrm{gd}^{-1}\theta+\sec\theta\tan\theta)+\pi(n+1)\mathrm{gd}^{-1}\theta$$
$$-\pi(n+1)(2n+\tfrac{1}{2})[\sec\theta\tan\theta+\ln\cos\theta-\ln(1-\sin\theta)]$$

$$+\mathrm{i}S(2n+\tfrac{3}{2})\tan^2\theta\}). \qquad (2.14)$$

Due to the $\mathcal{O}(\varepsilon S^3)$ correction term in (2.14), a secular behavior can be expected at large S. Since oscillations often occur at $S>10$, a WKB analysis will be more appropriate in practice.

2. The WKB Expansion

For large Strouhal numbers, $\sigma << 1$, and rapid oscillations occur on a short scale while a slow drift takes place on the scale $x=\mathcal{O}(1)$. The WKB ansatz can be formulized from

$$-\cos(\tfrac{\pi}{2}y)Y_n' + \mathrm{i}SY_n = 0\,,\ Y_n(0)=1\,,$$

or
$$Y_n = \exp(\tfrac{2}{\pi}\mathrm{i}S\mathrm{gd}^{-1}\theta). \qquad (2.15)$$

Setting $Y_n = g(y)\exp(\tfrac{2}{\pi}\mathrm{i}S\mathrm{gd}^{-1}\theta)$ and substituting back into (2.10) gives

$$g' + \left[\varepsilon S^3\cos^{-3}\theta + \pi(n+1)\tan\theta\right]g = \mathcal{O}(\varepsilon S^2). \qquad (2.16)$$

The leading-order WKB formulation, at $\mathcal{O}(\varepsilon S^2)$, can be obtained therefrom:

$$Y_n^0 = (\cos\theta)^{2n+2}\exp(\zeta_0 - \mathrm{i}\Phi_0)\,,$$

where

$$\zeta_0 = -\tfrac{1}{\pi}\xi(\mathrm{gd}^{-1}\theta + \sec\theta\tan\theta)\,,$$
$$\Phi_0 = -\tfrac{2}{\pi}S\mathrm{gd}^{-1}\theta\,. \qquad (2.17)$$

Here $\xi = \varepsilon S^3 = k^2\nu h v_w^{-3}$ controls the exponential rate of decay as $y\to 1$. The superscript in Y_n^0 refers to the zero order WKB expansion whose derivative automatically satisfies the remaining boundary condition at the core.

C. The Multiple Scale Approach

Following the approach described by Majdalani,[5] we introduce two independent virtual coordinates, $y_0 = y$, and $y_1 = \varepsilon s(y)$, where 's' is an undetermined scale function that we propose to find. Note that the proposed transformation represents a slight departure from conventional linear transformations bearing $y_1 = \delta(\varepsilon)y$. The current stipulation of y_1 offers the necessary freedom that will lead to a uniformly valid solution. As prescribed by multiple scale formalism, functions and derivatives can be expanded, following this virtual transformation, via

$$Y_n(y_0,y_1) = Y_0(y_0,y_1) + \varepsilon\, Y_1(y_0,y_1) + \mathcal{O}(\varepsilon^2)\,,$$
$$\frac{\mathrm{d}}{\mathrm{d}y} = \frac{\partial}{\partial y_0} + \varepsilon\frac{\mathrm{d}s}{\mathrm{d}y_0}\frac{\partial}{\partial y_1}\,,\ \frac{\mathrm{d}^2}{\mathrm{d}y^2} = \frac{\partial^2}{\partial {y_0}^2} + \mathcal{O}(\varepsilon). \qquad (2.18)$$

After substitution into (2.10), we segregate terms of the same order to arrive at the following set of coupled, partial differential equations

$$\frac{\partial Y_0}{\partial y_0} + \left[\frac{\pi}{2}(1+\lambda_n)\tan(\theta_0) - \mathrm{i}S\sec(\theta_0)\right]Y_0 = 0\,, \qquad (2.19)$$

$$\frac{\partial Y_1}{\partial y_0} + \left[\frac{\pi}{2}(1+\lambda_n)\tan(\theta_0) - \mathrm{i}S\sec(\theta_0)\right]Y_1 = -\frac{\mathrm{d}s}{\mathrm{d}y_0}\frac{\partial Y_0}{\partial y_1} + S\sec(\theta_0)\frac{\partial^2 Y_0}{\partial {y_0}^2}; \qquad (2.20)$$

where $\theta_0 = \tfrac{\pi}{2}y_0$. In much the same way, boundary conditions given by (2.11) can be converted into

$$Y_0(0) = 1\,,\ \frac{\partial Y_0}{\partial y_0}(1) = 0\,. \qquad (2.21)$$

Next we integrate (2.19) in a straightforward fashion to get

$$Y_0 = C_1\exp\left\{\ln(\cos\theta_0)^{1+\lambda_n} + \frac{2\mathrm{i}}{\pi}S\ln\tan\left[\frac{\pi}{4}(1+y_0)\right]\right\} \equiv C_1(y_1)\chi(y_0)\,, \qquad (2.22)$$

where C_1 is an integration function that must be determined in a manner to ensure a secular-free series expansion in Y_n. Differentiating (2.22), and plugging the results back into (2.20) gives

$$\frac{\partial Y_1}{\partial y_0} + \left[\frac{\pi}{2}(1+\lambda_n)\tan\theta_0 - \mathrm{i}S\sec\theta_0\right]Y_1 = \left\{-\frac{\mathrm{d}s}{\mathrm{d}y_0}\frac{\mathrm{d}C_1(y_1)}{\mathrm{d}y_1} + C_1(y_1)\sec\theta_0 \times\left[-S^3\sec^2\theta_0 + \frac{\pi^2}{4}(1+\lambda_n)(\lambda_n\tan^2\theta_0 - 1)S - \mathrm{i}\pi S^2\left(\frac{1}{2}+\lambda_n\right)\sec\theta_0\tan\theta_0\right]\right\}\chi(y_0)\,, \qquad (2.23)$$

Removing secular-producing terms demands that the right-hand side of (2.23) be *nil.* Otherwise, the asymptotic series will contain terms whose quotient between two successive orders can be unbounded. Fortunately, the resulting first-order differential equation in C_1 can be easily integrated in closed form. After reverting back to our laboratory coordinate, satisfaction of (2.21) furnishes

$$C_1(y) = \exp\left\{-\xi\left[\eta(y)\sec^3\theta - \eta(0)\right] + \xi\sigma^2\frac{\pi^2}{4} \times(1+\lambda_n)\left[\sec\theta\eta(y)(\lambda_n\tan^2\theta - 1) + \eta(0)\right] - \mathrm{i}\pi\xi\sigma\left(\frac{1}{2}+\lambda_n\right)\eta(y)\sec^2\theta\tan\theta\right\}, \qquad (2.24)$$

where the viscous parameter $\xi = \varepsilon S^3$ makes its appearance here along with the effective scale functional $\eta(y)$. The latter is defined by

$$\eta(y) \equiv s(y)/s'(y)\,. \qquad (2.25)$$

The leading-order term can now be summoned from (2.24) and (2.22) by gleaning knowledge from both zero and first order perturbation levels. In like fashion, further terms in the series of $\mathcal{O}(\varepsilon^2)$ can be obtained, but they become increasingly complicated, and one may wish to relinquish the effort to a symbolic program. Since the overall solution is sought at $\mathcal{O}(M)$, and $M > \varepsilon$, there is no justification for retaining other than Y_0, and the expansion in (2.18) reduces to

$$Y_n = (\cos\theta)^{1+\lambda_n} \exp\Big\{-\xi\Big[\eta\sec^3\theta - \eta(0)\Big] + \frac{\pi^2}{4S^2}\xi(1+\lambda_n) \times\Big[\eta\sec\theta(\lambda_n\tan^2\theta - 1) + \eta(0)\Big] + \tfrac{2}{\pi}\mathrm{i}S\mathrm{gd}^{-1}\theta - \mathrm{i}\pi\frac{\xi}{S}\left(\frac{1}{2}+\lambda_n\right)\eta\sec^2\theta\tan\theta\Big\} + \mathcal{O}(\varepsilon). \quad (2.26)$$

Obviously, the undetermined scale function remains, at present, unspecified. However, one can verify that, near the wall, an asymptotic solution exists for $s(y) = y$, as shown in detail by Majdalani.[5] Mathematically, this translates into

$$\lim_{y\to 0}\eta(y) = y \Rightarrow \eta(0) = 0, \quad (2.27)$$

which can be used to slightly simplify (2.26) before eventual substitution into (2.9). Note that this simplification is convenient but not necessary for the success of the current procedure. At the outset, we get

$$\tilde{u}(x,y,t) = -\mathrm{i}\cos\theta\sum_{n=0}^{\infty}\frac{(-1)^n(k_m x\cos\theta)^{2n+1}}{(2n+1)!} \times\exp\Big\{-\xi\eta\sec^3\theta\Big[1+\tfrac{\pi^2}{2}\sigma^2(n+1)(\cos 2\theta + 2n\sin^2\theta)\Big] + \tfrac{2}{\pi}\mathrm{i}S\ln\tan(\tfrac{\theta}{2}+\tfrac{\pi}{4}) - \mathrm{i}\pi\xi\sigma(2n+\tfrac{3}{2})\eta\sec^2\theta\tan\theta - \mathrm{i}k_m t\Big\} + \mathcal{O}(\varepsilon), \quad (2.28)$$

which is a rapidly converging series that displays distinctly terms of $\mathcal{O}(\sigma^2)$. In fact, the error associated with $n \geq 1$ terms can be verified to be smaller than the $\mathcal{O}(\varepsilon)$ entailed in the $n = 0$ term.

D. Closed-Form Solution

Careful examination of (2.28) reveals that a closed-form equivalent is possible when terms that do not affect the reported precision are dropped. This can be accomplished by dismissing the $\mathcal{O}(\sigma^2)$ quantities arising in the $n \geq 1$ terms. In practice, the equivalent expression reads

$$\tilde{u} = -\mathrm{i}\cos\theta\sin(k_m x\cos\theta)\exp\zeta\exp\Big[-\mathrm{i}(k_m t + \Phi)\Big] \quad (2.29)$$

where

$$\zeta = \zeta_0 + \zeta_1 = -\xi\eta\sec^3\theta - \tfrac{\pi^2}{2}\xi\sigma^2\eta\sec^3\theta\cos 2\theta, \quad (2.30)$$

and

$$\Phi = \Phi_0 + \Phi_1 = -\tfrac{2}{\pi}S\ln\tan(\tfrac{\theta}{2}+\tfrac{\pi}{4}) + \tfrac{3\pi}{2}\xi\sigma\eta\sec^2\theta\tan\theta \quad (2.31)$$

Clearly, each of the spatial damping function ζ and spatial phase angle Φ comprises a leading-order term and a small correction of $\mathcal{O}(\sigma^2)$.

E. Other Vortical Components

Having obtained an accurate expression for $\tilde{u}$, the transverse component $\tilde{v}$ can be extracted from mass conservation. To that end, we proceed heuristically by setting an *ansatz* of the form

$$\tilde{v} = G(y)\cos(k_m x\cos\theta)\exp\zeta\exp\Big[-\mathrm{i}(k_m t + \Phi)\Big], \quad (2.32)$$

where $G(y)$ is a subsidiary function that must be determined in a manner to satisfy continuity, namely, $\partial\tilde{u}/\partial x + \partial\tilde{v}/\partial y = 0$. After some algebraic operations, continuity is indeed fulfilled in leading-order quantities when $G = Mv_0^3$. Henceforth,

$$\tilde{v} = M\cos^3\theta\cos(k_m x\cos\theta)\exp\zeta\exp\Big[-\mathrm{i}(k_m t + \Phi)\Big] \quad (2.33)$$

indicating that our initial claim of $\tilde{v}/\tilde{u} = \mathcal{O}(M)$ was perfectly legitimate. Indubitably, this analytical realization can be verified numerically as well. Next in line, temporal vorticity can be issued directly from the velocity formulation. In fact, straightforward differentiation begets

$$\tilde{\omega}(x,y,t) = -S\sin(k_m x v_0)\exp\Big[\zeta - \mathrm{i}(k_m t + \Phi)\Big]. \quad (2.34)$$

F. Specifying the Undetermined Scale

1. *Velocity Consideration*

One may proceed by contending that the multiple scale formula should match, in leading order, the uniformly valid WKB expansion. This can be achieved by suppressing terms of $\mathcal{O}(\sigma^2)$ in (2.26) and equating the resulting expression to (2.17). At the outset, we find that

$$-\xi\eta\sec^3\theta = -\tfrac{1}{\pi}\xi(\mathrm{gd}^{-1}\theta + \sec\theta\tan\theta),$$

$$\text{or} \qquad \eta = \tfrac{1}{\pi}(\cos\theta\,\mathrm{gd}^{-1}\theta + \tan\theta)\cos^2\theta \quad (2.35)$$

From (2.25), one may solve for the appropriate scale function via $s' - \eta^{-1}s = 0$. Recalling that $s(0) = 0$, direct integration yields

$$s(y) = \exp\int_0^y \eta^{-1}(\tau)\mathrm{d}\tau = \sec(\tfrac{\pi}{2}y)\tan(\tfrac{\pi}{2}y) + \ln\tan\tfrac{\pi}{4}(1+y). \quad (2.36)$$

With this choice of s, the multiple scale solution given by (2.29) will coincide with the corresponding WKB formulation when $\zeta_1 = \Phi_1 = 0$. Retention of the first order

corrections ζ_1 and Φ_1 in (2.29) slightly increases the accuracy of the multiple scale formulation beyond its WKB counterpart.

2. Vorticity Consideration

The current expression for vorticity can be compared to its counterpart in Sec. V(F) of Paper I. Knowing that the exponential decay of time-dependent vorticity must be decreed by the same agents irrespective of the perturbation technique, the spatial damping function ζ must be the same as that obtained previously. This contention implies that, in (2.30), we must have

$$-\eta\sec^3(\tfrac{\pi}{2}y) = -\tfrac{1}{\pi}\Big[\ln\tan\tfrac{\pi}{4}(1+y) + \sec(\tfrac{\pi}{2}y)\tan(\tfrac{\pi}{2}y)\Big], \tag{2.37}$$

which leads to the same expressions obtained from velocity consideration.

3. Comparison with Previous Work

Fortuitously, we are able to manage, this time, an exact expression for the nonlinear transformation, $y_1 = \varepsilon s(y)$, that leads to a uniformly valid, multiple scale solution. Obviously, the complexity of formula (2.36) precludes the possibility of guessing this coordinate transformation beforehand, as demanded by conventional multiple scale procedures. It also justifies the need to deploy the 'reverse engineering' process in tracking the scales. The most striking result is, perhaps, the agreement between our current didactic formulation and the *ad hoc* formulation obtained by Majdalani[5] using a forward approach. In the previous analysis, a composite scale $s(y) = y(1-y)^{-3y^{3/2}/2}$ was constructed *ab initio* in a manner to reproduce asymptotically the inner, outer, and intermediate scales cropping up in the problem. As a result, usage of the composite scale reduced the number of spatial scales to two, which was necessary for the success of the multiple scale expansion. Subsequently, the effective scale functional η was derived and then substituted into the solution. In the current analysis, η is determined first, and only at the conclusion of the analysis that one may verify that the space-reductive coordinate does indeed reduce to the proper spatial scales in their regions of applicability. For instance, in the vicinity of the transpiring wall and core, one can recover the scales found by Majdalani.[5] Thus,

$$y_1 = \varepsilon\Big[\sec(\tfrac{\pi}{2}y)\tan(\tfrac{\pi}{2}y) + \ln\tan\tfrac{\pi}{4}(1+y)\Big] \to \{\varepsilon y\,,\ y\to 0, \quad \varepsilon(1-y)^{-2}\,,\ y\to 1\} \tag{2.38}$$

For the sake of illustration, η and s obtained herein are compared in Fig. 1 with their counterparts from Majdalani.[5] Clearly, predictions from the multiple scale solution agree in general form with those obtained previously using the composite scale technique.

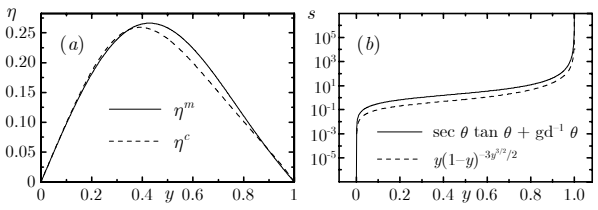

Fig. 1 Comparing the effective scale functional η in (a) and corresponding scale function s in (b) to existing composite scale results given by Majdalani.[5] Superscripts refer to 'multiple' or 'composite' scale solutions.

III. Results and Comparisons

A. The Oscillatory Velocity Profile

Since $\tilde{v}\,/\,\tilde{u} = \mathcal{O}(M)$, $\tilde{u}$ dominates the vortical description, and the total temporal velocity can be contrived by juxtaposition of irrotational and solenoidal fields. The result, from (2.29), is

$$u_1(x,y,t) = \mathrm{i}\big\{\sin(k_m x)\exp(-\mathrm{i}k_m t) - \cos\theta\sin(k_m x\cos\theta)\exp\Big[\zeta - \mathrm{i}(k_m t + \Phi)\Big]\big\}. \tag{3.1}$$

As Euler's notation is no longer needed, the real part of (3.1) can be retrieved into

$$u_1(x,y,t) = \overbrace{\sin(k_m x)\sin(k_m t)}^{\text{irrotational part}} - \overbrace{\underbrace{\cos\theta\sin(k_m x\cos\theta)\exp\zeta}_{\text{wave amplitude}}\ \underbrace{\sin(k_m t + \Phi)}_{\text{wave propagation}}}^{\text{rotational part}}. \tag{3.2}$$

In a sense, formula (3.2) is the apex of our labors. Clearly, the first term in (3.2) abbreviates the pressure-driven, inviscid response, and the second term represents the vorticity-driven, viscous response. In conformance with existing knowledge, formula (3.2) assumes a traditional constitution encountered in studies of periodic flows of the Stokes type, reminiscent of equation (10.3) in Rott.[6] As such, it vividly displays the vortical wave characteristics that permit exacting explicit formulations for the vortical depth of penetration, velocity overshoot, and surfaces of constant phase. Unlike theoretical studies that are concerned with infinitely long channels with oscillatory motions induced by pistons at infinity, a dependence on the axial coordinate x is brought about here by the body's finite length. Further examination of (3.2) reveals that the vortical

amplitude is decreed by two separate terms: an exponentially damped function owing to viscous dissipation, and a space-harmonic function made possible by inclusion of axial mean flow convection of vorticity fluctuations. Whereas both terms depreciate with increasing distance from the wall, the latter varies sinusoidally in the streamwise direction. Moreover, inspection of the spatial damping function ζ reveals that successive increases in viscosity promote vortical degeneration. This counterintuitive effect will be clarified below.

B. Comparison with Computational Data

In order to ascertain the validity of our asymptotics, we insist on comparisons with computational predictions. These are obtained from a dual time-stepping code, developed totally independently by Roh et al.[7] to manage the *nonlinearized* Navier-Stokes equations. The code is devoted to analyzing gas-phase processes based on the complete conservation equations of mass, momentum, and energy. Originally designed to treat propellant combustion in rocket motors, this implicit dual time-stepping integration method has proved its efficiency and robustness in reacting flows at all speeds. When launched, the algorithm invokes pressure decomposition and preconditioning techniques to circumvent difficulties encountered in low-speed compressible flows. Subsequently, the set of governing equations with appropriate boundary conditions is solved numerically by means of a finite-volume approach. A fully-coupled implicit formulation is then used to enhance numerical stability and efficiency. The scheme has the advantage of achieving a high degree of temporal accuracy with

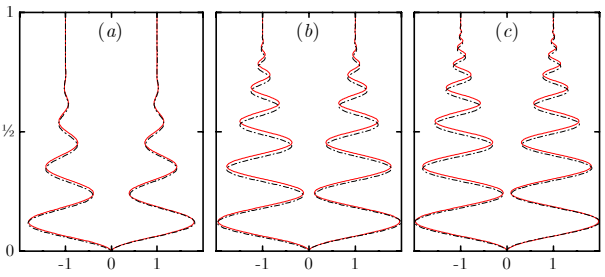

Fig. 2 Comparing the asymptotic solution (full curves) to numerical computations of the nonlinear Navier-Stokes equations (chain curves) at two successive times. Here $S = 25$, $x/l = ½$, and $m = 1$. Using a 40x300 mesh resolution, simulation results are shown after 9 iteration cycles for (a) $K = 10^4$, (b) $K = 10^5$, and (c) $K = 10^6$.

only a modest increase in computational cost. Moreover, since the governing equations are solved implicitly, the numerical method is very stable. As a result, the selection of the integration time step is dictated by the individual process, and not by numerical stability constraints.

For the same physical parameters employed in our asymptotic formulas, numerical simulations are monitored until convergence is ensured. This is done while keeping the number of binary places as high as possible in order to mitigate the machine's restriction to fixed-point arithmetic. The code relies on a uniform mesh resolution and therefore requires more points at higher Strouhal numbers to capture the depreciating vortical waves near the core. We find results obtained for a large number of test cases to be completely satisfactory.

For illustration purposes, we show in Fig. 2 both asymptotics and numerics at three orders of the kinetic Reynolds number. Cases corresponding to $K = 10^7$ and higher become nearly inviscid and bear a striking resemblance to Fig. 2(c). In every case, the velocity profiles, characterized by oscillations that progressively decay from the wall, are depicted at two successive times separated by a $\pi/2$ phase difference. The small disparity between theoretical and computational data can be attributed to small discretization errors and nonlinearity effects that elude our analytic formulation. This agreement is consistent at higher modes where an increasing number of cycles is required for convergence.

On that account, we show in Fig. 3 both asymptotic and computational predictions for $m = 2$ at the conclusion of several iteration cycles. After fifteen cycles, the discrepancy between theoretical and numerical experiments is hardly visible. In the absence of an exact solution to the case at hand, this comparison to a full Navier-Stokes solution is pivotal. Since the end justifies the means, it certainly gives our approach a 'raison d' être' by reconciling between our final analytical formulation and the nonlinear Navier-Stokes predictions.

C. Theoretical and Numerical Comparisons

In Table 1, we now compare numerical simulations of the *linearized* Navier-Stokes equations, described in Paper I, to the asymptotic results obtained from the multiple scale solution, given by (3.2), and the perturbation solution of Paper I. We select a test case with flow parameters that fall in the middle of the physical range under investigation. The last two columns

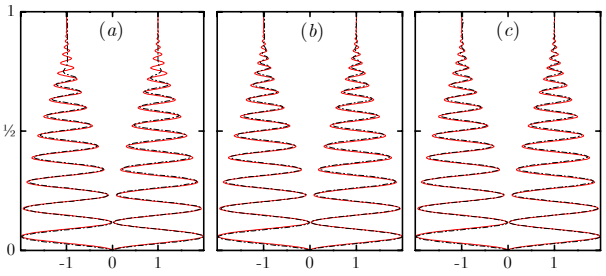

Fig. 3 Comparing the asymptotic solution (full curves) to numerical computations of the nonlinearized Navier-Stokes equations (chain curves) at two successive times. Here $K = 2\times10^6$, $S = 50$, $x/l = ¼$, and $m = 2$. Using a 40x300 mesh resolution, simulation results are shown after (*a*) 9, (*b*) 12, and (*c*) 15 iteration cycles.

give the percentage deviation of the preceding entries relative to the numerical approximations obtained with a high level of confidence. In fact, by observing the results at different tolerances and mesh sizes, the numerically reported data entries seem to be correct to all decimal places quoted. We have actually tested our numerical code on other differential equations that possess exact solutions. It is very satisfying to note the agreement, in many cases, to three or more decimal places, between our theoretical predictions and the corresponding numerical benchmark.

D. Wave Characteristics

For the purpose of confirming that our current formulation coincides with the perturbation solution of Paper I, the maximum velocity overshoot factor that occurs near the wall is quantified in Fig. 4. Practically, the calculated overshoot is the same, in both magnitude and location, irrespective of the formulation used. As discussed in Paper I, this phenomenon is a key feature of periodic flows that appears to be decidedly more significant in the presence of wall injection.

From (3.2), the normal speed of propagation of rotational waves, $\mathrm{d}y^*/\mathrm{d}t^*$, can be determined explicitly due to the compact formulation. The wave speed is thus found to match the steady flow velocity $(v_w v_0)$. As a result, the normalized spatial wavelength can be deduced to be $(2\pi v_0 / S)$, implying progressively diminishing vortical wavelengths near the core, where v_0 is small, and at high Strouhal numbers. This certainly explains our need to refine the computational mesh near the core to capture the rotational effects occurring at increasingly smaller length scales. It also confirms the slower convergence rate, borne out in Fig. 3, between theoretical and numerical predictions near the core.

Unlike its counterpart in Paper I, our formula permits defining the surfaces of constant phase in closed form. From the wave propagation term of (3.2), we read $\cos k_m(t+\Phi/k_m) = \text{const.}$, and reap, by way of the Gudermannian function, the equation for the characteristic surfaces at various c values, $y = \frac{4}{\pi}\arctan[\frac{\pi}{2}M(t-c)] - 1$.

Table 1 Oscillatory velocity predictions for $S = 50$, $K = 10^6$, $k_m t = \frac{\pi}{2}$, and $m = 1$

y	numeric	paper I asymp.	paper II asymp.	paper I error %	paper II error %
0.00	0.00000	0.00000	0.00000	0.00000	0.00000
0.05	1.79517	1.79519	1.79516	0.00105	0.00051
0.10	0.70421	0.70418	0.70430	0.00508	0.01227
0.15	0.73320	0.73323	0.73298	0.00376	0.02996
0.20	1.67981	1.67981	1.68009	0.00013	0.01683
0.25	0.14482	0.14480	0.14465	0.01650	0.11603
0.30	1.83552	1.83557	1.83541	0.00263	0.00610
0.35	0.27291	0.27282	0.27335	0.02991	0.16226
0.40	1.62642	1.62655	1.62574	0.00807	0.04205
0.45	0.42048	0.42031	0.42118	0.04276	0.16582
0.50	1.56396	1.56411	1.56364	0.00939	0.02037
0.55	0.53014	0.53030	0.52958	0.02991	0.10554
0.60	1.14062	1.13981	1.14204	0.07086	0.12412
0.65	1.27183	1.27244	1.27121	0.04772	0.04885
0.70	0.96405	0.96548	0.96323	0.14745	0.08547
0.75	0.93011	0.93169	0.92984	0.17065	0.02819
0.80	1.04257	1.04424	1.04280	0.16040	0.02256
0.85	0.98924	0.98734	0.98839	0.19249	0.08601
0.90	0.99654	0.99549	0.99582	0.10554	0.07238
0.95	0.99995	1.00001	1.00000	0.00546	0.00512
1.00	1.00000	1.00000	1.00000	0.00000	0.00000

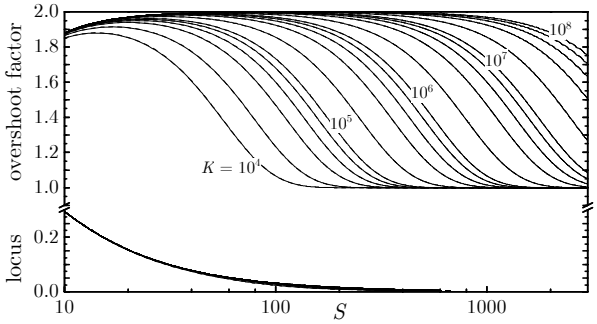

Fig. 4 For the first oscillation mode, we compare the Richardson velocity overshoot in both magnitude and location over a wide spectrum of physical parameters half way across the channel. To the accuracy of the graph, asymptotic results from Paper I (full curves) and Paper II (broken curves) are indistinguishable.

E. Penetration Depth

As explained in Sec. I, one would expect the shear layer to be pushed away from the wall and to approach the core asymptotically in R. Since it is nearly impossible to produce sharp estimates of the viscous layer thickness, we are inclined to focus, instead, on characterizing the penetration depth Δ of time-dependent rotational waves. We thus define Δ to be the normalized distance from the wall to the point where 99 percent of the rotational wave amplitude in (3.2) would have vanished. Since the viscous layer delineates two essentially inviscid zones, a rotational one near the wall, and an irrotational one near the core, Δ may serve to locate the blown-off layer as well. From (3.2), one can seize the point above the wall where the rotational amplitude reduces to $\alpha = 1$ percent of its irrotational counterpart. If $y = \Delta$ denotes such a point, then Δ is soluble from

$$\cos(\tfrac{\pi}{2}\Delta)\sin\left[k_m x\cos(\tfrac{\pi}{2}\Delta)\right]\exp\left[-\eta(\Delta)\xi\sec^3(\tfrac{\pi}{2}\Delta)\right] - \alpha\left|\sin(k_m x)\right| = 0. \qquad (3.3)$$

Despite its transcendental form, (3.3) indicates that the exponential decay is a strong function of a nondimensional penetration number, $\Lambda = \xi^{-1}$. This observation suggests generating curves of Δ versus Λ, for large variations in K and S. In fact, Fig. 5 shows how entire families of asymptotic curves over wide ranges of K and S collapse splendidly into single curves per axial position. Here too, asymptotics and numerics concur. This interesting result reveals that Δ does not depend on K and S separately, but rather on $\Lambda = KS^{-3}$, a parameter that resembles, in importance, the Stokes or Womersley numbers

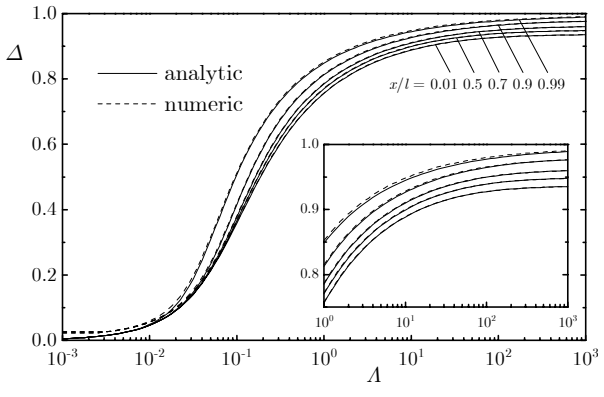

Fig. 5 Penetration depth for a wide range of parameters and axial locations including both numerical ($K = 10^6$) and asymptotic predictions ($10^4 < K < 10^8$). Part of the graph is enlarged in the inset.

in periodic flows over hard walls. Physically, it symbolizes the relative intensity of time-dependent inertia compared to viscous diffusion in the cross-streamwise direction. The pertinent ratio scales with

$$\frac{\text{Inertia}}{\text{Viscous force}} \approx \frac{\rho\frac{\partial v}{\partial t}}{\mu\frac{\partial^2 u}{\partial y^2}} \approx \frac{\rho\frac{v_w}{(1/k)}}{\mu\frac{kh}{(v_w/k)^2}} = \frac{v_w^3}{h\nu k^2} \equiv \Lambda. \qquad (3.4)$$

In a sense, Fig. 5 along with formula (3.3) bring into focus the character of the rotational penetration depth over permeable walls. For instance, it is clear that Δ depends on Λ, m and, to a lesser degree, on the axial station, especially within the aft portion of the channel. For small Λ, the penetration depth Δ varies linearly with the penetration number Λ, irrespective of x. Apparently, the larger the penetration number, the larger the penetration depth will be. This dimensionless grouping reveals that increasing injection, or decreasing viscosity, frequency, or channel height broadens the depth of penetration. Notably, our time-dependent solution represents a strongly damped wave whose penetration depth into the fluid is inversely proportional to ν. This is in sharp contrast to the depth of penetration of periodic flows over impermeable walls, where the dependence on the kinematic viscosity is the same as in boundary layer theory, namely, proportional to $\sqrt{\nu}$.

As borne out in the graph, for sufficiently large Λ, Δ approaches a maximum fixed value per axial station. In order to locate this maximum possible depth, $\Delta_\infty(m,x) = \Delta(\Lambda\to\infty, m, x)$, we realize that, for ideal fluids, rotational waves face minimum resistance and, thereby, travel the furthest distance from the wall. The asymptotic limit can thus be evaluated from the inviscid formulation of the penetration depth —which only relies on the axial station and pressure oscillation mode. From (3.3), we read

$$\cos(\tfrac{\pi}{2}\Delta_\infty)\sin\left[k_m x\cos(\tfrac{\pi}{2}\Delta_\infty)\right] - \alpha\left|\sin(k_m x)\right| = 0, \qquad (3.5)$$

which possesses an accurate asymptotic expansion with a maximum absolute error of 2.62×10^{-4}. The error occurs at the smallest possible value of $\Delta_\infty(1,0) = 0.9364$. This formula,

$$\Delta_\infty = 1 - \tfrac{2}{\pi}\sqrt{\alpha\left|\sin(k_m x)\right|k_m^{-1}x^{-1}} + \mathcal{O}(1-\Delta_\infty)^3, \qquad (3.6)$$

can be used in exchange for the numerical solution of (3.5), being correct to $\mathcal{O}(10^{-4})$.

F. Asymptotic Error Behavior

To gain further reassurance, we retrace our footsteps from Paper I by analyzing the maximum

absolute error between numerics and asymptotics. In much the same way, we again calculate the maximum difference E_{m} between formula (3.2) and the corresponding numerical solution of the linearized equations. Results are shown in Fig. 6 at several discrete values of the Strouhal number. We also compare our current error to that incurred previously in Paper I. As one can infer from the graph, the error approaches ε rapidly as $\varepsilon \to 0$. Also, there is a slight improvement in the maximum error associated with the multiple scale formulation. Overall, both remain at $\mathcal{O}(\varepsilon)$.

IV. Concluding Remarks

In this paper, we have presented an accurate formulation to the periodic flow in a channel with porous walls. The adopted strategy led to considerable mathematical simplifications and physical clarity. In addition to extracting closed-form expressions for a number of flow parameters, the results revealed interesting physical quantities that appear in the problem. Comparisons with computational data acquired from linearized and nonlinearized Navier-Stokes solvers were gratifying. Another substantial raison d'être for this paper was to provide dual verifications that lend support to the overall method used, and to previously developed formulations.

The interesting mathematical aspect of this investigation, that could possibly be extended to other practical problems, is the way in which the inclusion of an undetermined scale precipitates the scaling transformation needed to arrive at a uniformly valid solution. We hope that the space-reductive ideas addressed heretofore be exploited in other physical settings involving a multiplicity of spatial scales.

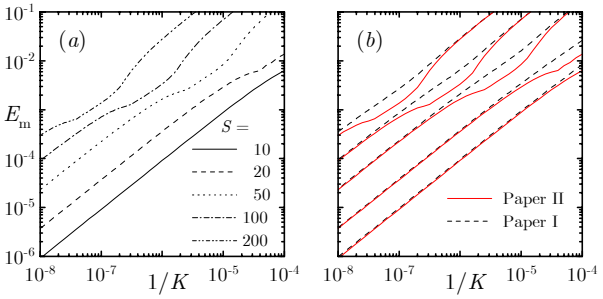

Fig. 6 Maximum absolute error entailed in (*a*) the multiple scale solution of Paper II, and (*b*) both asymptotic solutions of Papers I and II.

References

[1]Proudman, I., "An Example of Steady Laminar Flow at Large Reynolds Number," *Journal of Fluid Mechanics,* Vol. 9, No. 4, 1960, pp. 593-612.

[2]Catherall, D., Stewartson, K., and Williams, P. G., "Viscous Flow Past a Flat Plate with Uniform Injection," *Proceedings of the Royal Society, London, Series A,* Vol. 284, 1965, pp. 370-396.

[3]Cole, J. D., and Aroesty, J., "The Blowhard Problem - Inviscid Flows with Surface Injection," *International Journal of Heat and Mass Transfer,* Vol. 11, No. 7, 1968, pp. 1167-1183.

[4]Terrill, R. M., "Laminar Flow in a Uniformly Porous Channel with Large Injection," *The Aeronautical Quarterly,* Vol. 16, 1965, pp. 323-332.

[5]Majdalani, J., "A Hybrid Multiple Scale Procedure for Boundary Layers Involving Several Dissimilar Scales," *Zeitschrift für angewandte Mathematik und Physik,* Vol. 49, No. 6, 1998, pp. 849-868.

[6]Rott, N., *Theory of Time-Dependent Laminar Flows*, *High Speed Aerodynamics and Jet Propulsion –Theory of Laminar Flows*, Sec. D, Vol. IV, edited by F. K. Moore, Princeton University Press, Princeton, New Jersey, 1964, pp. 395-438.

[7]Roh, T. S., Tseng, I. S., and Yang, V., "Effects of Acoustic Oscillations on Flame Dynamics of Homogeneous Propellants in Rocket Motors," *Journal of Propulsion and Power,* Vol. 11, No. 4, 1995, pp. 640-650.